Enhancement of Förster energy transfer from thermally activated delayed fluorophores layer to ultrathin phosphor layer for high color stability in non-doped hybrid white organic light-emitting devices*

Zijun Wang(王子君)[1], Juan Zhao(赵娟)[2,†], Chang Zhou(周畅)[1], Yige Qi(祁一歌)[1], and Junsheng Yu(于军胜)[1,‡]

[1] *State Key Laboratory of Electronic Thin Films and Integrated Devices, School of Optoelectronic Information, University of Electronic Science and Technology of China (UESTC), Chengdu* 610054, *China*

[2] *School of Chemistry, Sun Yat-sen University, Guangzhou* 510275, *China*

(Received 16 December 2016; revised manuscript received 29 December 2016; published online 20 February 2017)

Fluorescence/phosphorescence hybrid white organic light-emitting devices (WOLEDs) based on double emitting layers (EMLs) with high color stability are fabricated. The simplified EMLs consist of a non-doped blue thermally activated delayed fluorescence (TADF) layer using 9,9-dimethyl-9,10-dihydroacridine-diphenylsulfone (DMAC-DPS) and an ultrathin non-doped yellow phosphorescence layer employing bis[2-(4-tertbutylphenyl)benzothiazolato-N,C2'] iridium (acetylacetonate) ($(tbt)_2Ir(acac)$). Two kinds of materials of 4,7-diphenyl-1,10-phenanthroline (Bphen) and 1,3,5-tris(2-N-phenylbenzimidazolyl) benzene (TPBi) are selected as the electron transporting layer (ETL), and the thickness of yellow EML is adjusted to optimize device performance. The device based on a 0.3-nm-thick yellow EML and Bphen exhibits high color stability with a slight Commission International de l'Eclairage (CIE) coordinates variation of (0.017, 0.009) at a luminance ranging from 52 cd/m^2 to 6998 cd/m^2. The TPBi-based device yields a high efficiency with a maximum external quantum efficiency (EQE), current efficiency, and power efficiency of 10%, 21.1 cd/A, and 21.3 lm/W, respectively. The ultrathin yellow EML suppresses hole trapping and short-radius Dexter energy transfer, so that Förster energy transfer (FRET) from DMAC-DPS to $(tbt)_2Ir(acac)$ is dominant, which is beneficial to keep the color stable. The employment of TPBi with higher triplet excited state effectively alleviates the triplet exciton quenching by ETL to improve device efficiency.

Keywords: white organic light-emitting devices, non-doped emitting layers, thermally activated delayed fluorescence, color stability

PACS: 73.21.Ac, 78.60.Fi, 85.60.Jb, 73.61.Ph **DOI:** 10.1088/1674-1056/26/4/047302

1. Introduction

White organic light-emitting devices (WOLEDs) have great potential applications in displays and solid-state lighting,[1–6] owing to their favorable properties, such as high efficiency, high resolution, and potential realization on flexible substrates. To obtain highly efficient WOLEDs, a key requirement is that all electrically generated excitons, i.e., both singlet and triplet excitons, must be employed for radiative decay.[7,8] During the past few decades, various approaches to fully harness excitons have been raised. Phosphorescent WOLEDs have shown very high efficiencies, owing to the theoretical 100% internal quantum efficiency of the phosphorescent emitters. However, these devices are limited by the lack of high-performance blue emitters, which are not stable to ensure a long device life-time.[9] With the purpose of generating highly efficient and stable white light, hybrid WOLEDs adopting blue fluorescent materials and green/red or yellow phosphorescent materials have been widely employed, due to excellent stability of fluorophores and high efficiency of phosphors. Generally speaking, to achieve high quantum efficiency for hybrid WOLEDs, mutual quenching between fluorescent and phosphorescent materials should be prevented. One common strategy is to insert an interlayer between the fluorescence and phosphorescence emissive layers (EMLs) to reduce the triplet loss on the blue emitter because of its low and non-radiative triplet state (T_1).[1,10,11] However, using an interlayer has numerous disadvantages that will limit the device quantum efficiency and power efficiency, besides, the additional fabrication step for an interlayer will cause an adverse impact on the commercial applications.[12] Under the conditions that use blue fluorophores with high T_1, even if the triplet excitons are trapped by blue fluorophores, they can still be transferred to the phosphors with lower T_1, which can still achieve 100% internal quantum efficiency in such devices.[13,14] Therefore, the interlayer can be avoided. Zhang and Lee *et al.* demonstrated hybrid WOLEDs with a max external quantum efficiency (EQE) of 21% and a low turn-on voltage of 3.4 V em-

*Project supported by the National Natural Science Foundation of China (Grant Nos. 61675041 and 61605253), the Foundation for Innovation Research Groups of the National Natural Science Foundation of China (Grant No. 61421002), and the Science & Technology Department Program of Sichuan Province, China (Grant No. 2016HH0027).

†Corresponding author. E-mail: zhaoj95@mail.sysu.edu.cn

‡Corresponding author. E-mail: jsyu@uestc.edu.cn

© 2017 Chinese Physical Society and IOP Publishing Ltd

ploying new blue fluorophores with high T_1.[14] Though these surpass the blue conventional fluorophores with high T_1, there still exists a problem that the emission spectra have to be adjusted carefully, as the singlet excitons created in blue fluorophores can be transferred to phosphors resulting in insufficient blue emission, which is required for balanced white light, because triplet excitons cannot be used by blue phosphors.[12]

Currently, a remarkable breakthrough on the thermally activated delayed fluorescence (TADF) materials by Adachi and co-workers affords a new way to make the more efficient blue fluorophores with high T_1 practicable.[15,16] Blue TADF fluorophores can allow both electro-generated singlet and triplet excitons light emission through thermal upconversion of the lowest T_1 to singlet state (S_1) since the energy gap between S_1 and T_1 (ΔE_{ST}) is sufficiently small, which leads to the potential for achieving 100% internal emission efficiency.[17–19] Moreover, the recycling of triplet excitons can realize an adequate blue fluorescent emission, which can match better with yellow or red/green emission to obtain high performance hybrid WOLEDs. Therefore, hybrid WOLEDs using blue TADF fluorophores can further simplify the structure and reduce the triplet loss, which is superior to these using conventional blue fluorophores with high T_1. Usually, blue TADF materials are doped into the host materials to decrease triplet exciton quenching.[20] However, among problems with doping methods is the difficulty of control of the relative guest–host doping concentration accurately and selecting a host whose energy level matches well with the dopants. These problems have been more complicated in hybrid WOLEDs, as doping in each EML needs to be optimized separately for balanced white emission and improved efficiency.[21] To loosen the bottlenecks of doping method, the non-doped technology is practically helpful. As a number of studies reported, non-doped OLEDs can be free of any kind of doping through all the function layers, which results in a simple manufacturing process and an excellent reproducibility.[22–24] Both non-doped all-fluorescent WOLEDs[25] and non-doped all-phosphorescent WOLEDs[21,26] have been reported. However, so far, little work on the non-doped hybrid WOLEDs has been carried out.

In this work, we propose an easily realized strategy to fabricate highly efficient hybrid WOLEDs. The hybrid WOLEDs based on non-doped EMLs with high efficiency have been designed by employing a blue TADF emitter and a yellow phosphorescence emitter. The blue TADF emitter consisting of a kind of blue TADF fluorophores 9,9-dimethyl-9,10-dihydroacridine-diphenylsulfone (DMAC-DPS) that is insensitive to the doping ratio and exhibits high quantum efficiency has been reported,[27,28] and hybrid WOLEDs using DMAC-DPS as blue fluorophores have already exhibited high performance.[29,30] So, pure DMAC-DPS can be used as blue EML for non-doped hybrid WOLED, which affords an effective way to realize high performance, and has merits of simplified fabrication process, repeatability improvement, and cost reduction.

2. Experimental detail

Indium tin oxide (ITO) coated glass substrates with a sheet resistance of 10 Ω/sq were cleaned in an ultrasonic bath with detergent water, acetone, deionized water, and isopropyl alcohol, respectively. Pre-cleaned ITO was treated with oxygen plasma under a pressure of 25 Pa for 5 min after it was dried in nitrogen gas flow. The organic functional layer and metallic cathode were subsequently deposited without breaking the vacuum, while keeping the pressure of the order of magnitude 10^{-4} Pa and 10^{-3} Pa, respectively. The deposition rate and the thickness of the thin films were in situ monitored using a quartz crystal oscillator mounted to the substrate holder. The organics and metal oxide were evaporated at the rate of 1 Å/s except that the evaporation rate of ultrathin layer is 0.05 Å/s, and the metals were evaporated at the rate in a range 9 Å/s–11 Å/s. The overlap between ITO and Mg:Ag electrodes was 0.2 cm^2, which is the active emissive area of the devices. The current density–voltage–luminance (J–V–L) characteristics were tested with a Keithley 4200 source and a luminance meter. Both electroluminescence (EL) spectra and CIE coordinates of the devices were recorded with a spectrophotometer OPT-2000. All the measurements were performed in air at room temperature without encapsulation.

The fabricated hybrid WOLED structure was given as: ITO/MoO_3 (8 nm)/TAPC (40 nm)/mCP (10 nm)/DMAC-DPS (10 nm)/$(tbt)_2$Ir(acac) (X nm)/Bphen (40 nm)/Mg:Ag (100 nm). Therein, to reduce the operating voltage, molybdenum trioxide (MoO_3) was used as the hole injecting layer, while 1,1-bis((di-4-tolylamino)phenyl) cyclohexane (TAPC), 3,5'-N,N'-dicarbazole-benzene (mCP), and 4,7-diphenyl-1,10-phenanthroline (Bphen) were employed as the hole transporting layer (HTL), exciton blocking layer (EBL) and electron transporting layer (ETL). Pure DMAC-DPS acted as blue EML while ultrathin bis[2-(4-tertbutylphenyl)benzothiazolato-N,C2'] iridium (acetylacetonate) ($(tbt)_2$Ir(acac)) was used as yellow EML, where X nm represents 0.1 nm, 0.3 nm, 0.5 nm, and 0.7 nm for device W1, device W2, device W3, and device W4, respectively. The ultrathin $(tbt)_2$Ir(acac) layer forms partial film which can be considered as a dope-type device in which the $(tbt)_2$Ir(acac) is doped into DMAC-DPS and Bphen simultaneously in a low doping concentration.[31] Figure 1 shows the molecular structures of materials used and the energy level diagram of the device. DMAC-DPS has a highest occupied molecular orbital (HOMO) energy level of 5.9 eV along with a lowest unoccupied molecular orbital (LUMO) energy level of 2.9 eV,[29] which is the same as that of mCP and Bphen, respectively.

These matched energy levels, which are responsible for the low turn-on voltage of all the devices, can promote charge carrier transport into the EMLs, but the hole transport through the TAPC HTL prior to transport across the mCP EBL, and the electron transport across the Bphen ETL. Moreover, DMAC-DPS has bipolar charge transfer property due to the 9, 9-dimethyl-9, 10-dihydroacridine (DMAC) donor, and diphenylsulfone (DPS) acceptor groups in its chemical structure as shown from Fig. 1(b), which facilitates both holes and electrons to transport and recombine in the EMLs.

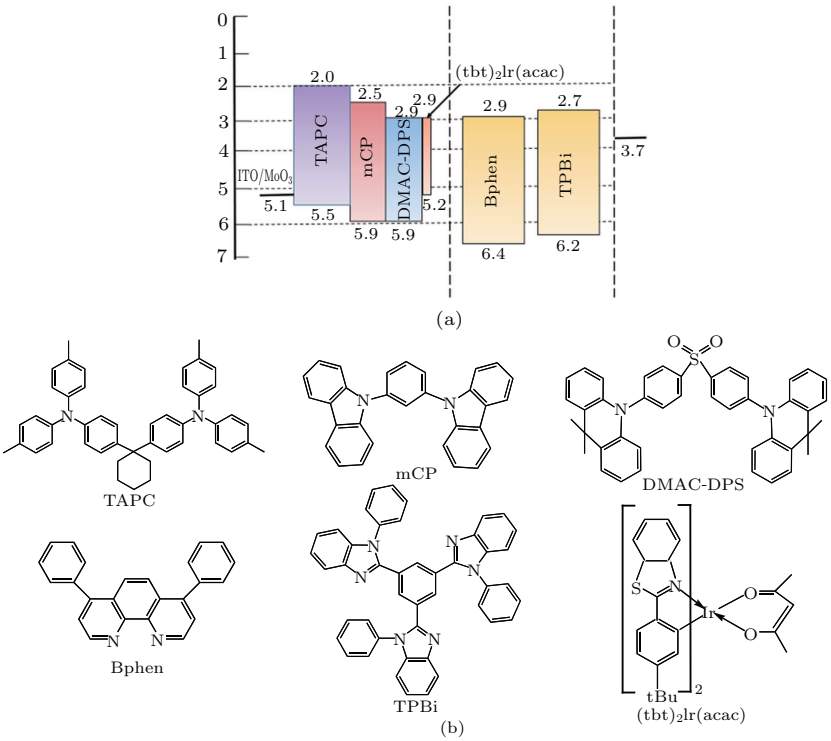


Fig. 1. (color online) (a) Schematic energy level diagram of the WOLEDs. (b) Chemical structures of used materials.

3. Results and discussion

The thickness of $(tbt)_2Ir(acac)$ is increased from 0.1 nm to 0.7 nm in order to adjust the ratio of blue emission to yellow emission so as to obtain white emission and optimize device performance. Figure 2(a) shows the *J*–*V*–*L* characteristics of the devices W1–W4. We find that *J*–*V* curves of devices with increasing the thickness of $(tbt)_2Ir(acac)$ from 0.1 nm, 0.3 nm, 0.5 nm, to 0.7 nm are almost overlapped. It means that the current density is independent on $(tbt)_2Ir(acac)$ layer thickness. If a decreased current density is observed when the thickness of $(tbt)_2Ir(acac)$ layer is increased, the emission mechanism is dominated by charge trapping and direct exciton formation, since the emitters will trap charge carriers and change the current density. On the other hand, if there is little influence of layer thickness on the *J*–*V* characteristics, the charge trapping effect may be limited.[23,32] Although the HOMO of $(tbt)_2Ir(acac)$ is shallower than DMAC-DPS and Bphen, the hole-trapping effect on yellow ultrathin EML is negligible. So, the independence of *J*–*V* curves on the dye concentration means that host-guest energy transfer dominates the main emission mechanism of devices W1–W4. Table 1 summarizes the power efficiency (*PE*, lm/W), current efficiency (*CE*, cd/A), and *EQE* (%) characteristics of devices from Fig. 2. As we can see, device W2 with optimized thickness of 0.3 nm $(tbt)_2Ir(acac)$, which has the highest luminance of 8273 cd/m^2, has maximum current efficiency of 21.7 cd/A, power efficiency of 25.7 lm/W, and *EQE* of 6.8%.

The energy transfer and white light emission process of devices W1–W4 are described schematically in Fig. 3. Specifically, these processes can be discussed as follows: (i) under electrical excitation, the excitons are formed in DMAC-DPS. (ii) As mentioned above, energy transfer dominates the emission process in devices W1–W4. To DMAC-DPS, firstly, prompt fluorescent is generated by deactivation of the directly formed S_1 state to the ground state (GS). Then, the T_1 state can be up-converted into S_1 state via reverse intersystem crossing (RISC) because of a small ΔE_{ST}, causing the delayed fluorescence. (iii) The S_1 energy of the DMAC-DPS is transferred to $(tbt)_2Ir(acac)$ through Förster energy transfer (FRET). The T_1 energy of the DMAC-DPS almost cannot be transferred to the T_1 of $(tbt)_2Ir(acac)$ with Dexter energy transfer, because Dexter energy transfer can be blocked by increasing the distance between the donor and the acceptor molecule, which is caused by the thin $(tbt)_2Ir(acac)$ layer.[32,33] (iv) Energy transition for the yellow phosphor happens from the S_1 state to T_1 state at a high rate of speed through spin–orbit coupling (SOC) induced by the heavy metal effect,[34] and yellow phosphorescence is emitted by relaxation of the T_1 state to the GS.

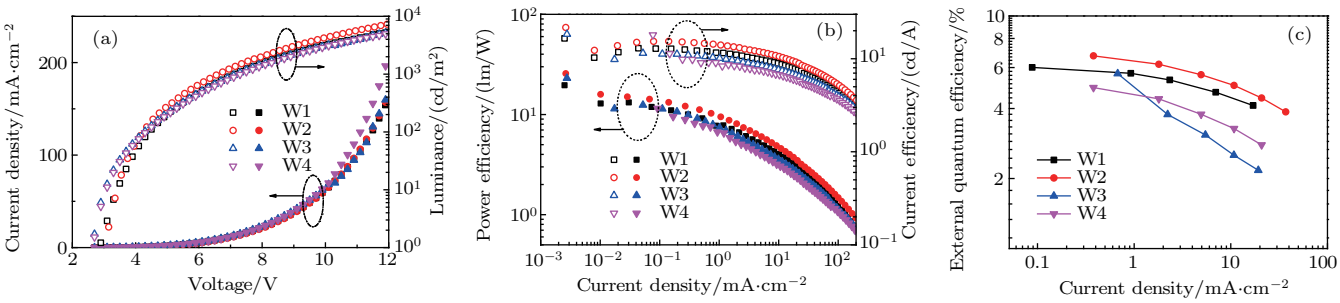


Fig. 2. (color online) (a) Current density–voltage–luminance (*J*–*V*–*L*) characteristics of devices W1–W4. (b) Power efficiency–current density–current efficiency (*PE*–*J*–*CE*) characteristics of the devices W1–W4. (c) External quantum efficiency–current density (*EQE*–*J*) characteristics of the devices W1–W4.

Table 1. EL characteristics of devices W1–W5.

Devices	Turn-on voltage/V	Max. *L*/(cd/m^2)	Max. *CE*/(lm/W)	Max. *PE*/(cd/A)	Max. *EQE*/%	CIE@(100, 1000, and 5000 cd/m^2)
W1	2.8	6314	19.6	16.5	6.1	(0.26, 0.35) (0.26, 0.34) (0.27, 0.34)
W2	2.8	8273	25.7	21.7	6.8	(0.31, 0.40) (0.32, 0.41) (0.32,0.40)
W3	2.7	6184	23.1	18.4	6.0	(0.27, 0.36) (0.31, 0.39) (0.34, 0.40)
W4	2.7	5825	18.8	18.1	5.5	(0.31, 0.38) (0.33, 0.39) (0.36, 0.42)
W5	3.1	9377	21.3	21.1	10.0	(0.38, 0.43) (0.43, 0.45) (0.44, 0.45)

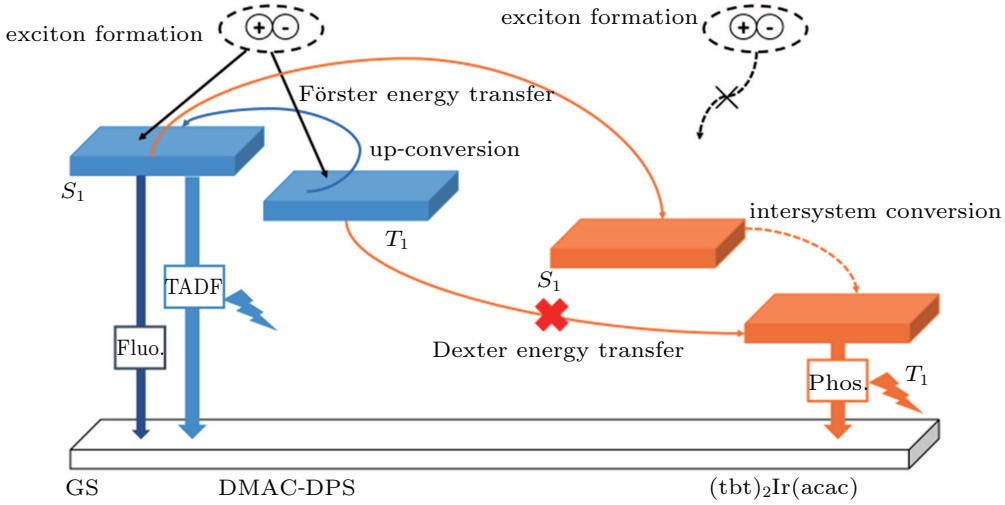


Fig. 3. (color online) Energy transfer and light emission process of devices W1–W4.

When taking practical applications into account, excellent color stability is as crucially important as high efficiency for the WOLED. The normalized EL spectra of the four devices W1–W4 at different voltage are shown in Figs. 4(a)–4(d). It is clearly seen that the yellow emission at 552-nm peak and 600-nm shoulder is originated from (tbt)$_2$Ir(acac), while the blue emission peak at 470 nm is originated from non-doped DMAC-DPS. The four devices show CIE of (0.25, 0.34), (0.32, 0.41), (0.31, 0.39), and (0.33, 0.39) at a luminance of 1000 cd/m^2, respectively. As we can see, it is of great interest to note that devices W1 and W2 exhibit excellent color-stability, showing no significant dependence on the drive voltage. Device W2 with CIE coordinates of (0.32, 0.41) exhibits excellent spectra stability with negligible shift in CIE coordinates of (0.017, 0.009) when the luminance increases from 52 cd/m^2 to 6998 cd/m^2, which is probably due to the saturation of FRET from DMAC-DPS layer to (tbt)$_2$Ir(acac) layer even in low voltage with thinner yellow layer. However, for devices W3 and W4, the intensity of yellow emission sharply increases relative to the blue emission with the voltage increasing. With relatively thicker yellow layer, the FRET from DMAC-DPS to (tbt)$_2$Ir(acac) is not sufficient at low voltage, and rises to saturation with the increasing voltage. It is the reason why yellow emission increases with the voltage increasing in devices W3 and W4.

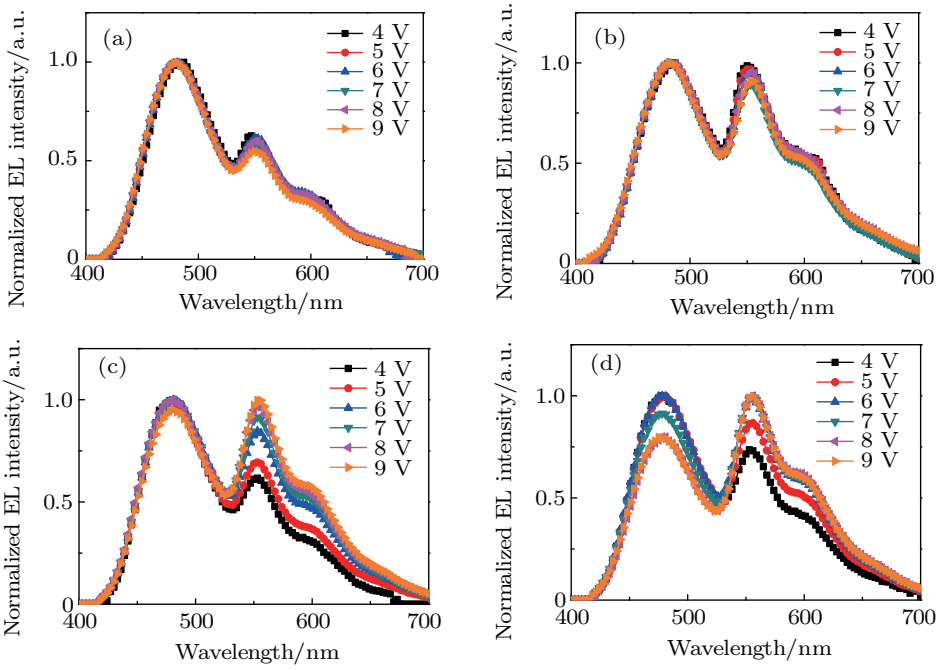


Fig. 4. (color online) EL spectra of device (a) W1, (b) W2, (c) W3, (d) W4. The unit a.u. is short for arb. units.

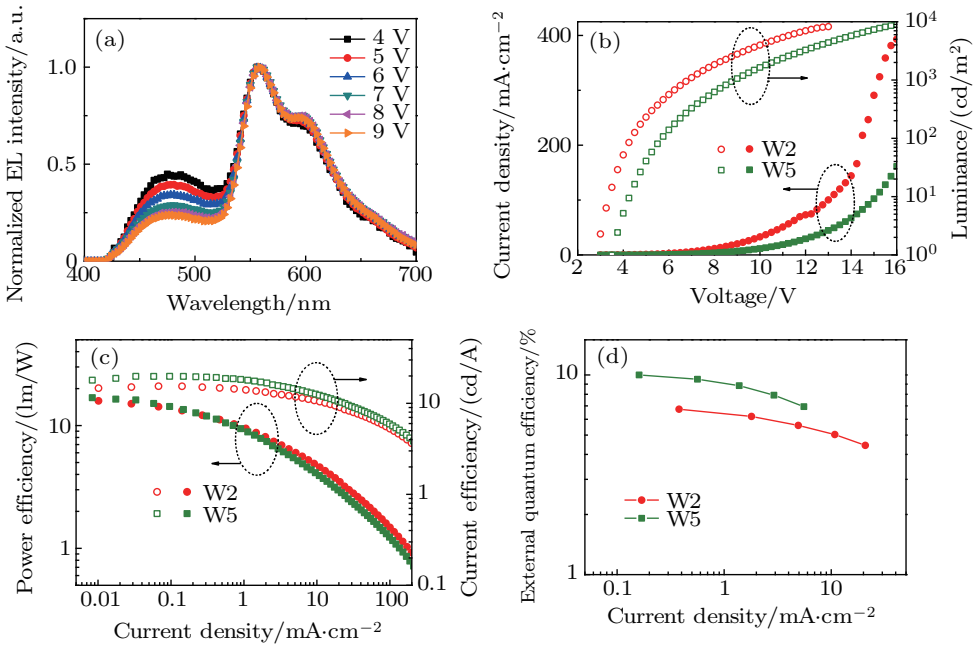


Fig. 5. (color online) (a) EL spectra of device W5 at various biases. (b) *J*–*V*–*L* characteristics of devices W2 and W5. (c) *PE*–*J*–*CE* characteristics of the devices W2 and W5. (d) *EQE*–*J* characteristics of the devices W2 and W5.

Considering that DMAC-DPS has a T_1 of 2.7 eV,[29] TAPC with a T_1 of 2.87 eV is adopted as the HTL and mCP with a T_1 of 2.9 eV[35] is used as the EBL. Although Bphen ETL exhibits a higher T_1 of 2.5 eV[36] than that of $(tbt)_2Ir(acac)$ ($T_1 = 2.2$ eV),[37] it is still lower than that of DMAC-DPS. We assume that the mediocre performance of Bphen devices is probably due to the excitons formed in DMAC-DPS partly diffusing into the Bphen ETL and quenching with the cathode.[38] To investigate the effect of ETL on the device performance, TPBi was used as the ETL and EBL since it has higher T_1 and relatively decent electron mobility in device W5, wherein the configuration was given as: ITO/MoO_3 (8 nm)/TAPC (40 nm)/mCP (10 nm)/DMAC-DPS(10 nm)/$(tbt)_2Ir(acac)$(0.3 nm)/TPBi (40 nm)/Mg:Ag (100 nm). Figure 5 shows the EL spectra at different voltages and the comparison of electrical characteristics between Bphen device and TPBi device. We had found that, with 0.3 nm $(tbt)_2Ir(acac)$, W5 has maximum *CE* of 21.1 cd/A, *PE* of 21.3 lm/W and *EQE* of 10% from Table 1. In addition to the electron mobility of TPBi ($\sim 3.3 \times 10^{-5}$ cm^2·V^{-1}·s^{-1})[39]

being lower than that of Bphen ($\sim 10^{-4}$ cm$^2\cdot$V$^{-1}\cdot$s^{-1}),[36] it can be seen from Fig. 1 that the electron injection barrier from cathode to TPBi (1 eV) is higher than that to Bphen (0.8 eV), so the turn-on voltage of W5 (3.1 V) as shown in Fig. 5(b) is higher than that of W2 (2.8 V), which is in agreement with the lower power efficiency of W5.

To further investigate the effect of different electron transporting materials on electrical performance of the hybrid WOLEDs, EQE characteristics are studied. The formulas we used to calculate the EQE are taken from previous work by Suzuki,[40] and the external quantum efficiency (η_{ex}) can be expressed as Eq. (1)

$$\eta_{ex} = \frac{N_p}{N_e}, \tag{1}$$

where N_p is the number of photons emitted externally from the hybrid WOLED devices and N_e is the number of electrons injected into it within unit time. N_p can be obtained from the measured luminance and EL spectrum, which can be expressed as Eq. (2)

$$N_p = \pi \cdot A \int_{380}^{780} \frac{I(\lambda)\cdot\lambda}{683\cdot hc}\,\mathrm{d}\lambda, \tag{2}$$

where λ is the wavelength, and $I(\lambda)$ is the relative EL intensity at each wavelength. h is the Planck constant, and c is the velocity of light. N_e is related to current I_e (A) flowing into the hybrid WOLED devices and can be expressed as Eq. (3)

$$N_e = \frac{I_e}{e}\ (\mathrm{s}^{-1}), \tag{3}$$

where e is the electron charge. From Eqs. (1), (2), and (3), maximum EQE of devices have been calculated, which are shown in Fig. 5(d). Compared with W2, the maximum EQE has been improved by 50% in device W5. In addition, TPBi has a T_1 of 2.8 eV,[39] which is higher than that of both DMAC-DPS and $(tbt)_2$Ir(acac), so the formed excitons can be well confined in the DMAC-DPS and $(tbt)_2$Ir(acac) EMLs rather than diffusion into the ETL, and energy loss can be effectively avoided. By increasing the applied voltage from 4 V to 9 V, as learned from Fig. 5(a) the blue intensity is slightly decreased, and the CIE coordinates of the devices range from (0.38, 0.43) to (0.43, 0.45), and warm white emission is obtained. Thus, it can further prove that high-efficiency hybrid WOLEDs could be obtained by using a non-doped structure.

4. Conclusion

In summary, we have fabricated simplified hybrid WOLEDs with non-doped EMLs consisting of a blue TADF EML and an ultrathin yellow phosphorescent EML. The DMAC-DPS with concentration independent property enables itself to act as a highly efficient non-doped EML. Meanwhile, its bipolar transport property is beneficial to broaden charge recombination zone. The thickness of ultrathin $(tbt)_2$Ir(acac) layer has influences on not only EL spectra stability, but also luminance characteristics and efficiencies via FRET. A maximum PE and CE of 25.7 lm/W and 21.7 cd/A, respectively, have been achieved by the optimized $(tbt)_2$Ir(acac) thickness of 0.3 nm, along with almost stable CIE coordinate of (0.32, 0.41) from 52 cd/m^2 to 6998 cd/m^2. As Bphen is replaced by TPBi as ETL material, the device obtains a highest maximum EQE of 10%, since TPBi with higher T_1 can block excitons diffusing into ETL. The results indicate that the blue TADF emitter DMAC-DPS could be an effective alternative to replace the conventional blue fluorophores in hybrid WOLEDs, which can simplify device fabrication and improve reproducibility. This work provides a new applicable route for developing high-performance WOLEDs.

References

[1] Sun Y, Giebink N C, Kanno H, Ma B, Thompson M E and Forrest S R 2006 *Nature* **440** 908
[2] Kido J, Kimura M and Nagai K 1995 *Science* **267** 1332
[3] Jou J H, Hsieh C Y, Tseng J R, Peng S H, Jou Y C, Hong J H, Shen S M, Tang M C, Chen P C and Lin C H 2013 *Adv. Funct. Mater.* **23** 2750
[4] He Z S, Yu H M, Peng H and Hou X Y 2015 *Chin. Phys. B* **24** 097201
[5] Liu B Q, Tao H, Su Y J, Gao D Y, Lan L F, Zou J H and Peng J B 2013 *Chin. Phys. B* **22** 077303
[6] Reineke S, Lindner F, Schwartz G, Seidler N, Walzer. K, Lussem B and Leo K 2009 *Nature* **459** 234
[7] Wang C, Li X L, Pan Y Y, Zhang S T, Yao L, Bai Q, Li W J, Liu P, Yang B, Su S J and Ma Y G 2016 *ACS Appl. Mater. Interfaces* **8** 3041
[8] Liu X K, Chen Z, Zheng C J, Chen M, Liu W and Zhang X H 2015 *Adv. Mater.* **27** 2025
[9] Zhang Y F, Lee J S and Forrest S R 2014 *Nat. Commun.* **5** 5008
[10] Zhao F C, Zhang Z Q, Liu Y P, Dai Y, Chen J S and Ma D G 2012 *Org. Electron.* **13** 1049
[11] Zheng C J, Wang J, Ye J, Lo M F, Liu K Q and Fung M K 2013 *Adv. Mater.* **25** 2205.
[12] Sun N, Wang Q, Zhao Y B, Chen Y H, Yang D Z, Zhao F C, Chen J S and Ma D G 2014 *Adv. Mater.* **26** 1617
[13] Ye J, Zheng C, Ou X M, Zhang X H, Fung M K and Lee C S 2012 *Adv. Mater.* **24** 3410
[14] Zheng C J, Wang J, Ye J, Lo M F, Liu K Q, Fung M K, Zhang X H and Lee C S 2013 *Adv. Mater.* **25** 2205
[15] Endo A, Ogasawara M, Takahashi A, Yokoyama D, Kato Y and Adachi C 2009 *Adv. Mater.* **21** 4802
[16] Uoyama H, Goushi K, Shizu K, Nomura H and Adachi C 2012 *Nature* **492** 234
[17] Nishide J, Nakanotani H, Hiraga Y and Adachi C 2014 *Appl. Phys. Lett.* **104** 233304
[18] Kim B S and Lee J Y 2015 *Org. Electron.* **21** 100
[19] Higuchi T, Nakanotani H and Adachi C 2015 *Adv. Mater.* **27** 2019
[20] Sun J W, Kim K W, Moon C K, Lee J H and Kim J J 2016 *ACS Appl. Mater. Interfaces* **8** 9806
[21] Wang Q, Oswald I W H, Perez M R, Jia H, Shahub A A, Qiao Q, Gnade B E and Omary M A 2014 *Adv. Funct. Mater.* **24** 4746
[22] Yin Y M, Yu J, Cao H T, Zhang L T, Sun H Z and Xie W F 2014 *Sci. Rep.* **4** 6754
[23] Xue K W, Han G G, Duan Y, Chen P, Yang Y Q, Yang D, Duan Y H, Wang X and Zhao Y 2015 *Org. Electron.* **18** 84

[24] Xue K W, Sheng R, Chen B Y, Duan Y, Chen P and Yang Y Q, Wang X, Duan Y H and Zhao Y 2015 *RSC Adv.* **5** 39097
[25] Yang H 2013 *J. Lumin.* **142** 231
[26] Zhao Y, Chen J and Ma D 2013 *ACS Appl. Mater. Interfaces* **5** 965
[27] Zhang Q S, Li B, Huang S P, Nomura H, Tanaka H and Adachi C 2014 *Nat. Photon.* **8** 326
[28] Zhang Q S, Tsang D, Kuwabara H, Hatae Y, Li B, Takahashi T, Lee S Y, Yasuda T and Adachi C 2015 *Adv. Mater.* **27** 2096
[29] Zhang D D, Cai M G, Zhang Y G, Zhang D Q and Duan L 2015 *ACS Appl. Mater. Interfaces* **7** 28693
[30] Song W and Lee J Y 2015 *J. Phys. D: Appl. Phys.* **48** 365106
[31] Su Z S, Li W L, Xu M L, Li T L, Wang D, Su W M, Niu J H, He H, Zhu J Z and Chu B 2007 *J. Phys. D: Appl. Phys.* **40** 2783
[32] Wang X, Wang R, Zhou D and Yu J S 2016 *Synth. Metals* **214** 50
[33] Zhang D D, Duan L, Li C, Li Y L, Li H Y, Zhang D Q and Qiu Y 2014 *Adv. Mater.* **26** 5050.
[34] Lee C W, Renaud C, Rendu P Le, Nguyen T P, Seneclauze B, Ziessel R, Kanaan H and Jolinat P 2010 *Solid State Sci.* **12** 1873
[35] Eom S H, Zheng Y, Wrzesniewski E, Lee J, Chopra, So F and Xue J G 2009 *Appl. Phys. Lett.* **94** 153303
[36] Lee J H, Huang C L, Hsiao C H, Leung M K, Yang C C and Chao C C 2009 *Appl. Phys. Lett.* **94** 223301
[37] Zhao J, Yu J S, Liu S Q and Jiang Y D 2012 *J. Lumin.* **132** 1994
[38] Kang Y J and Lee J Y 2016 *Org. Electron.* **32** 109
[39] Hung W Y, Ke T H, Lin Y T, Wu C C, Hung T H, Chao T C, Wong K T and Wu C I 2006 *Appl. Phys. Lett.* **88** 064102
[40] Okamoto S, Tanaka K, Izumi Y, Adachi H, Yamaji T and Suzuki T 2001 *Jpn. J. Appl. Phys.* **40** (part 2, No.7B) L783